Mathematical Biosciences and Engineering

MBE, 20 (2): 1599–1616.
DOI: 10.3934/mbe.2023073
Received: 1 June 2022
Revised: 13 October 2022
Accepted: 20 October 2022
Published: 03 November 2022

http://www.aimspress.com/journal/MBE

Research article

Adaptive fuzzy-based stability control and series impedance correction for the grid-tied inverter

Sue Wang[1], Chaohong Zhou[1,2], Saleem Riaz[3], Xuanchen Guo[4], Haider Zaman[5], Alsharef Mohammad[6], Ahmad Aziz Al-Ahmadi[6], Yasser Mohammed Alharbi[6] and NasimUllah[6,*]

[1] School of Electrical and Control Engineering, Shaanxi University of Science and Technology, Xi'an 710021, China
[2] Changqing Oilfield Clean Power Development Project Department, Xi'an 710021, China
[3] School of Automation, Northwestern Polytechnical University, Xi'an 710072, China
[4] The Second Oil Extraction Plant of Changqing Oilfield Company, Qing'yang 745100, China
[5] Electronics Engineering Department, University of Engineering and Technology Peshawar, Khyber, PakhtunKhwa, Pakistan
[6] Department of Electrical Engineering College of Engineering, TAIF University, TAIF, 21944, Saudi Arabia

***Correspondence:** Email: nasimullah@tu.edu.sa, 1906011@sust.edu.cn.

Abstract: The regenerative braking in the tram allows the energy to be returned to the power grid through a power inverter. Since the inverter location between the tram and the power grid is not fixed, resulting in a wide variety of impedance networks at grid coupling points, posing a severe threat to the stable operation of the grid-tied inverter (GTI). By independently changing the loop characteristics of the GTI, the adaptive fuzzy PI controller (AFPIC) can adjust according to different impedance network parameters. It is challenging to fulfill the stability margin requirements of GTI under high network impedance since the PI controller has phase lag characteristics. A correction method of series virtual impedance is proposed, which connects the inductive link in a series configuration with the inverter output impedance, correcting the inverter equivalent output impedance from resistance-capacitance to resistance-inductance and improving the system stability margin. Feedforward control is adopted to improve the system's gain in the low-frequency band. Finally, the specific series impedance parameters are obtained by determining the maximum network impedance and setting the minimum phase margin of 45°. The realization of virtual impedance is simulated by conversion to an equivalent control block diagram, and the effectiveness and feasibility of the proposed method are verified by simulation and a 1 kW experimental prototype.

Keywords: grid-tied inverter (GTI); impedance network; adaptive fuzzy PI controller (AFPIC); series impedance correction; stability margin

1. Introduction

A power converter connects the tram to the power grid, facilitating bidirectional power flow [1]. During the normal tram operation, the converter operates as a rectifier. In braking, the converter operates in the inverter mode, feeding back the braking energy to the power grid [2]. However, there is no fixed point for the interface point between the tram and the grid. Therefore, a wide range of impedance networks is possible on the grid side, changing with the connection point [3], especially when the impedance network is large; it seriously affects the control loop gain of the GTI system during tram braking, resulting in system instability [4].

According to [5], in GTI, a significant number of nonlinear equipment is linked to the grid side. When the tram braking energy feeding back to the grid, it is necessary to ensure both the stability of DC side voltage and the good quality of grid current, requiring the GTI to have good steady-state performance. In [6], detecting DC side voltage gives the reference value of the AC side network access current. By controlling the DC side voltage and AC side current, the system has good stability in the braking energy feedback process. In [7], the authors proposed a method using small-signal modeling to analyze the relationship between converter output impedance and DC side line impedance and employing the virtual impedance method to improve the stability of the converter system. Most scholars consider the stability of DC side voltage, reasonable power flow distribution, and power compensation for braking energy feedback to the grid. However, the network impedance at the power grid side changes in real-time due to the different positions of trams connected to the grid while braking. When the network impedance is large, the power grid presents weak inductance, resulting in the decline of the stability margin of the GTI system. Therefore, it is necessary to consider the stability of the GTI system under the condition of a high impedance network.

The combination of fuzzy control and PI control can effectively improve the performance of inverter under strong current network or low network impedance. For example, [8] uses a double fuzzy PI controller to improve the performance of the inverter, in which the input of the main fuzzy controller is the voltage error and the variation of the error, and the output of the main fuzzy controller is used to adjust the parameters of the PI controller; The input of the sub fuzzy controller is the given voltage change on the DC side and the voltage change on the AC side of the inverter, and the output of the sub fuzzy controller is used to assist in adjusting the parameters of the PI controller. This double fuzzy control method effectively reduces the impact on the stability of the inverter system when the DC side voltage changes in a wide range, and also effectively improves the dynamic response speed of the system. [9] Proposed a fuzzy proportional complex integral control (PCI) method to eliminate the control error caused by specific frequency interference signal, suppress the high-order harmonic of grid connected current and improve the quality of grid connected current. [10] introduces an improved ZVS-PWM inverter, which uses fuzzy control to simulate the action mechanism of PID to reduce the complexity of the system. Compared with traditional PID control, PID-like fuzzy controller using fuzzy control to simulate PID working mechanism has better robustness. For islanding solar grid coupled inverters, [11] suggested an adaptive fuzzy control approach. The unmodelled section of a solar grid-connected inverter is simulated using fuzzy control, which decreases the control system's dependency on the model and increases the controller's accuracy. A fuzzy PI composite controller is proposed in [12]. In

comparison to classical PI control, fuzzy control updates PI settings live, effectively eliminating DC side voltage overshoot and improving the system's dynamic response speed. [13] combines the fuzzy-logic-based PI controller and the sliding mode controller. The fuzzy controller is connected in series with the PI controller to adjust the PI controller parameters online, which improves the stability of the system. The output of the PI controller is used as the input of the sliding mode controller, which effectively improves the dynamic response speed of the system. Compared with the traditional PI, the proposed method effectively ensures the dynamic performance and steady-state performance of the system, the sensitivity of the system to parameter changes is reduced. In [14], AFPIC is deployed to substitute PI voltage outer loop control, which enhances the robustness of the system and reduces the overshoot of the system. At the same time, the output voltage is feed forward to the input, which effectively weakens the impact of DC side voltage in the start-up stage and increases the anti-disturbance capability of the converter. [15] Designs and implements a GTI based on fuzzy PI control. The parameters of PI controller are adaptively adjusted through control, so that the system can obtain better starting effect and quickly recover to a stable state in case of disturbance.

The above literature shows that AFPIC can effectively improve the stable operation, dynamic response speed, tracking performance and robustness of the inverter. However, under the background of weak grid [16,17], the network impedance of different coupling points is different, resulting in the network impedance of inverter access point is not fixed [18,19], especially the high network impedance will seriously affect the gain of control loop, resulting in the reduction of phase margin, poor stability and poor performance of GTI[20,21]. At the same time, due to the inherent phase lag characteristics of PI controller, it is difficult to take into account the dynamic performance and steady-state performance of the system when adjusting PI controller parameters online[22]. In GTI system, PI controller also has parameter stability range, and fuzzy controller can not adjust PI controller parameters without limit. Therefore, under the condition of high network impedance, it is difficult to meet the stability margin requirements of GTI system only by adjusting PI controller parameters online through fuzzy control. [23]analyzed the impact of phase-locked loop (PLL) and inner loop control bandwidth on the stability margin of MMC system under different short circuit ratio (SCR).Connecting a VSC-HVDC link to a very weak grid (a high-impedance grid) is challenging. [24] Proposes and compares two straightforward solutions, through analysis and comparison, the method to ensure the good stability of the system is obtained.

In order to solve the problem of insufficient stability margin of AFPIC under the condition of high network impedance, a control strategy of fuzzy adaptive PI and series impedance correction is proposed in this paper. The output impedance of the inverter is connected in series with the inductive virtual impedance, so that the output impedance of the inverter is corrected from resistive capacitance to resistive inductance. The relevant series virtual impedance characteristics are determined using bode diagram analysis and the specified line impedance and minimum phase margin. Finally, through the equivalent transformation of the control block diagram, the realization of the virtual impedance is simulated in the control, the phase margin of the output impedance of the inverter under the condition of high network impedance is improved, and the amplitude gain of the low-frequency band of the system is improved through feed forward control. The combination of impedance correction and feed forward control makes the AFPIC have good control performance in all frequency bands.

This research work categorized and divided into five sections. In the second section, the model of GTI under weak current network is established, and the reason for insufficient stability margin of AFPIC under high network impedance is explained. The third section introduces how to use

impedance correction method to improve the stability margin of fuzzy adaptive PI control, and how to use feed forward control to improve the amplitude gain of low frequency band. The fifth section verifies the effectiveness of the proposed method through simulation and experiments, and the fourth section summarizes the article.

2. Methods

2.1. AFPIC of GTI in weak current network

Fuzzy adaptive PI control is often used to analyze nonlinear systems because of its good dynamic response ability. At present, many scholars have applied fuzzy adaptive PI control to photovoltaic grid connected inverter.

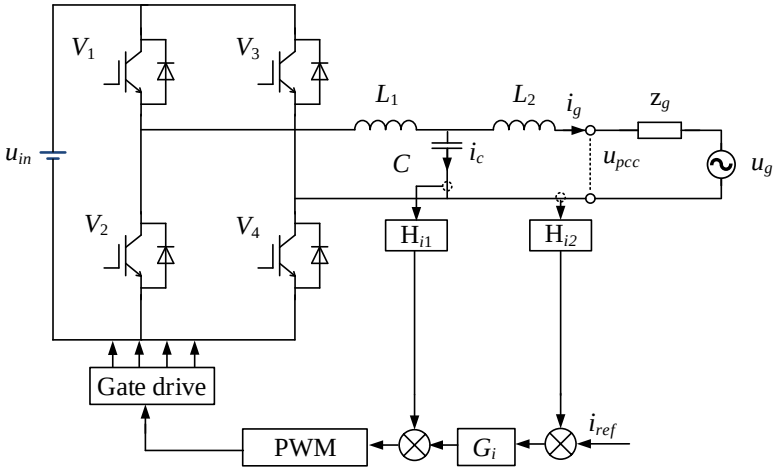

Figure 1. Main topology and control structure of LCL inverter.

The topology and control structure of the GTI are shown in Figure 1, in which u_{in} is the DC input voltage, V_1、V_2、V_3 and V_4 are the switches, L_1, C and L_2 constitute the LCL filter, z_g is the network impedance, u_g is the grid voltage, i_c is the capacitive current, i_g is the grid access current, u_{pcc} is the coupling point voltage, i_{ref} is the reference current, H_{i1} and H_{i2} are the feedback coefficients of capacitive current and grid access current respectively. And Figure 2 is the control block diagram of GTI.

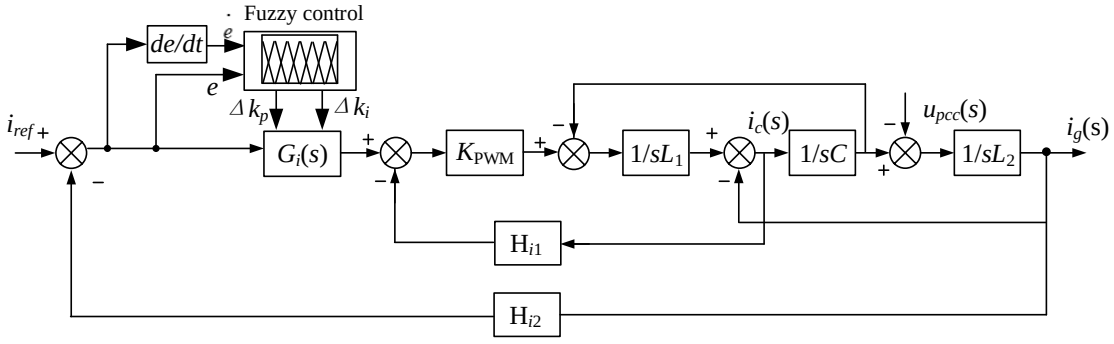

Figure 2. Control block diagram.

$$G_i(s) = K_{\mathrm{p}} + \frac{K_{\mathrm{i}}}{s} \tag{1}$$

where K_p、K_i is as

$$\begin{cases} K_{\mathrm{p}} = K_{p0} + \Delta k_p \\ K_{\mathrm{i}} = K_{i0} + \Delta k_i \end{cases} \tag{2}$$

K_{p0} and K_{i0} are the initial parameters of PI controller, Δk_p and Δk_i is the adjustment amount of K_{p} and K_{i}. The deviation e and deviation change rate $\dot{e}$ between the reference current i_{ref} and the network access current i_g are used as the input of the fuzzy controller, Δk_p and Δk_i are used as the output of the fuzzy controller.

The tuning rules are established based on experience, mainly considering the influence of PI controller parameters on stability, dynamic performance and steady-state performance.
The table of fuzzy control rules is shown in Table 1.

Table 1. Δk_p、Δk_i fuzzy control rule.

$\Delta k_p/\Delta k_i$		$\dot{e}$						
		NB	NM	NS	ZO	PS	PM	PB
	NB	PB|NB	PB|NB	PM|NB	PM|NM	PS|NM	PS|ZO	ZO|ZO
	NM	PB|NB	PB|NB	PM|NM	PM|NM	PS|NS	ZO|ZO	ZO|ZO
	NS	PM|NM	PM|NM	PM|NS	PS|NS	ZO|ZO	NS|PS	NM|PS
e	ZO	PM|NM	PS|NS	PS|NS	ZO|ZO	NS|PS	NM|PS	NM|PM
	PS	PS|NS	PS|NS	ZO|ZO	NS|PS	NS|PS	NM|PM	NM|PM
	PM	ZO|ZO	ZO|ZO	NS|PS	NM|PM	NM|PM	NM|PB	NB|PB
	PB	ZO|ZO	NS|ZO	NS|PS	NM|PM	NM|PB	NB|PB	NB|PB

1) When the current error e is large, in order to quickly reduce error and improve the system response speed, K_{p} takes the larger value and K_{i} takes the smaller value or zero; With the decrease of deviation e, in order to prevent oscillation caused by excessive overshoot, K_{p} should be lowered, and K_{i} should be taken as the smaller value; When the deviation e is very small, K_{p} value shall continue to decrease, and K_{i} value shall remain unchanged or be larger to eliminate the static error and avoid the oscillation of the system near the reference value.

2) The larger the change rate of current deviation, the smaller the value of K_{p} and the larger the value of K_{i}.

3) When the current deviance e and its rate $\dot{e}$ both have positive or negative signs, the incoming current changes in the direction of deviation from the reference current, simultaneously, the control function should be strengthened to make the deviation change towards the decreasing trend. We can take smaller K_{i} which should be taken; When the positive and negative signs of e and $\dot{e}$ are different, it indicates that the incoming current changes towards the direction close to the reference current. When the current deviation e is large, take a smaller K_{p} to speed up the transient response. Figure 3 can be obtained by equivalent transformation of Figure 2, Figure 3 is further transformed to Figure 4.

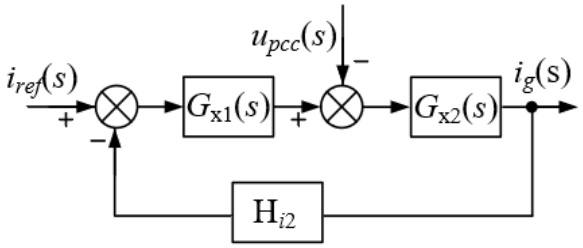

Figure 3. Equivalent transformation diagram.

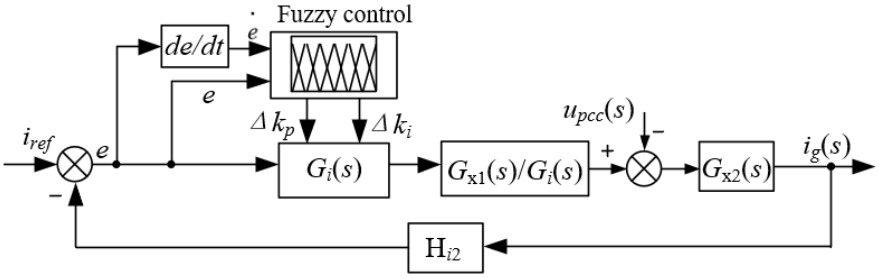

Figure 4. Structure diagram of fuzzy adaptive PI control.

$G_{x1}(s)$ and $G_{x2}(s)$ can be expressed as

$$G_{x1}(s) = \frac{K_{PWM}}{s^2 L_1 C + sCH_{i1}K_{PWM} + 1} G_i(s) \tag{3}$$

$$G_{x2}(s) = \frac{s^2 L_1 C + sCH_{i1}K_{PWM} + 1}{s^3 L_1 L_2 C + s^2 L_2 CH_{i1}K_{PWM} + s(L_1 + L_2)} \tag{4}$$

L_1, L_2 and C are LCL filter parameters, and K_{PWM} is modulation coefficient. Inverter loop gain is as follow:

$$T(s) = G_{x1}(s)G_{x2}(s)H_{i2}(s) \tag{5}$$

According to the national grid connection standard, the short-circuit ratio (SCR) less than 10 can be called weak network [25], and the calculation of transmission line impedance is:

$$L_g = \frac{u_g}{\mathrm{SCR} \times 2\pi \times f \times i_g} \tag{6}$$

where f is the grid frequency, u_g is the grid voltage and i_g is the grid current.

When SCR = 10 and i_g = 50A, L_g=1.4mH. As shown in Figure 5, when SCR >1 0, although the phase decreases with the increase of inductance, it can still meet the requirement that the phase margin is greater than 45°. However, when L_g = 1.4mH (SCR = 10), the stability margin of GTI decreases to 9°, which is far less than the requirements of GTI for stability margin. We can clearly observe that the AFPIC has limited regulation ability, it can only ensure the good stability of the system under low network impedance. When the network impedance is large, the AFPIC has poor stability or even loses stability.

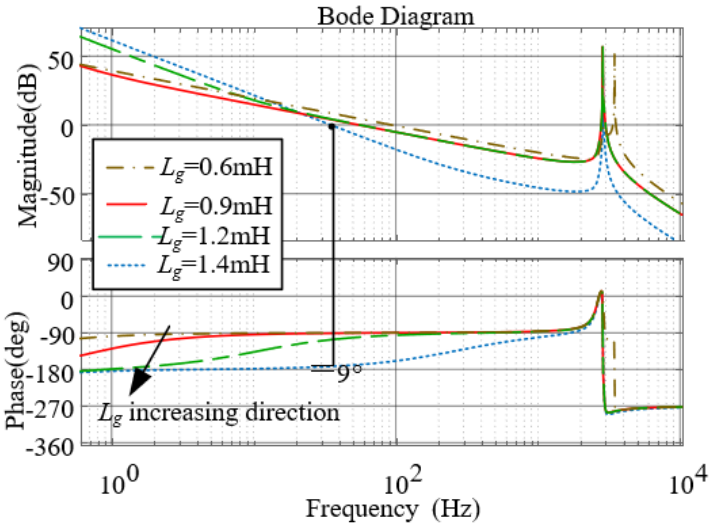

Figure 5. Stability margin of GTI for different impedance.

2.2. Series impedance correction method of inverter

2.2.1. Series impedance correction

To raise the stability margin of AFPIC under high network impedance, the method of series virtual impedance is adopted. In order to analyze the output, we should assume that the output impedance of the inverter is equivalent.

According to Figure 3 and Eqs (3)–(5), the network access current can be expressed as

$$i_g = \frac{1}{H_{i2}} \times \frac{\Gamma(s)}{1+\Gamma(s)} \cdot i_{ref}(s) - \frac{G_{x2}}{1+\Gamma(s)} \cdot u_{pcc}(s) \tag{7}$$

with (7), $i_s(s)$ and Z_{inv} is as follow:

$$i_s(s) = \frac{1}{H_{i2}} \times \frac{\Gamma(s)}{1+\Gamma(s)} \cdot i_{ref}(s) \tag{8}$$

$$Z_{inv}(s) = \frac{1+\Gamma(s)}{G_{x2}(s)} \tag{9}$$

It can be concluded from Eqs (7)–(9), that the inverter can be represented as a parallel combination of current source $i_s(s)$ and output impedance $Z_{inv}(s)$, as illustrated in Figure 6.

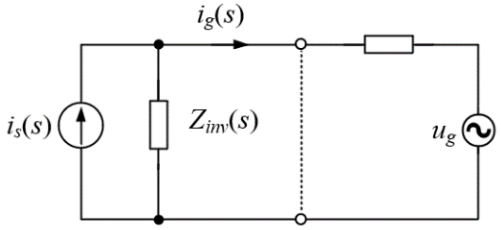

Figure 6. Equivalent diagram of inverter output impedance.

The grid side current is given by relation

$$\begin{aligned} i_g &= \frac{Z_{inv}(\mathrm{s})}{Z_{inv}(\mathrm{s})+Z_g(\mathrm{s})} i_s(s) - \frac{1}{Z_{inv}(\mathrm{s})+Z_g(\mathrm{s})} u_g(\mathrm{s}) \\ &= \left(i_s(\mathrm{s}) - \frac{u_g(\mathrm{s})}{Z_{inv}(\mathrm{s})} \right) \cdot \frac{1}{1+\dfrac{Z_g(\mathrm{s})}{Z_{inv}(\mathrm{s})}} \end{aligned} \tag{10}$$

Let H_1 and H_2 be the following equations respectively:

$$H_1 = i_s(\mathrm{s}) - \frac{u_g(\mathrm{s})}{Z_{inv}(\mathrm{s})} \tag{11}$$

$$H_2 = \frac{1}{1+\dfrac{Z_g(\mathrm{s})}{Z_{inv}(\mathrm{s})}} \tag{12}$$

The stability of the system depends on H_1 and H_2. Since H_1 is only related to the inverter parameters, the phase margin of H_1 can be regarded as a fixed value. Therefore, H_2 determines whether the system is stable or not. Following are the two conditions that must be met to ensure the stability of GTI,

1) The GTI is stable when the line impedance Zg = 0
2) $1+Z_g/Z_{inv} = 0$ is stable.

Condition 1 can be satisfied by the parameter design of the inverter, and condition 2 can be analyzed by using the frequency stability criterion, that is, at the intersection frequency of Z_g and Z_{inv}, the phase margin of the system is PM > 0. The calculation formula of system phase margin PM at intersection frequency is as follow:

$$\mathrm{PM} = 180^{\circ} - [\arg(Z_g(\mathrm{j}\omega)) - \arg Z_{inv}(\mathrm{j}\omega)] \tag{13}$$

ω is the intersection frequency of Z_g and Z_{inv}.

We can clearly observe from Eq (13) that the stability margin of the system can be improved by increasing the phase of Z_{inv}, and the series impedance correction can effectively improve the phase margin of Z_{inv}. The equivalent output impedance of inverter after series impedance correction is shown in Figure 7, the equivalent output impedance of the inverter is as follow:

$$Z = Z_{inv} + Z_{o3} \tag{14}$$

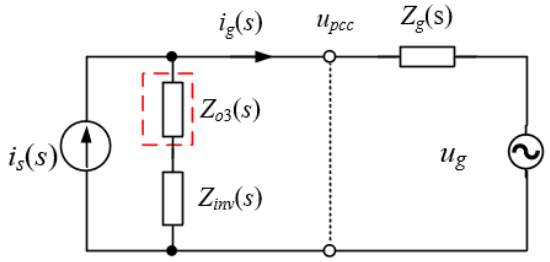

Figure 7. Series impedance correction equivalent circuit.

The equivalent output impedance of the inverter is resistance capacitance in most frequency bands, as displayed in Figure 8. Therefore, the output impedance can be corrected from resistance capacitance to resistance inductance by connecting the resistance inductance impedance Z_{o3} in series. After series correction, the phase of equivalent output impedance Z can be greatly improved.

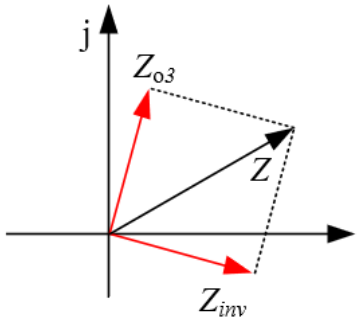

Figure 8. Impedance vector diagram.

Z_{o3} is as follow:

$$Z_{o3} = L_3 s + R_3 \tag{15}$$

We can clearly observe from Figure 8 that the larger L_3, the more obvious the phase increase of Z_{inv}. Therefore, the series pure inductive impedance is most conducive to improve the phase margin. SCR = 3 is chosen, considering the design of the series virtual impedance under the weak power grid. Use iterative method to continuously increase L_3 until PM > 45° is met. Take the phase margin PM = 45°, and the corresponding L_3 = 750 uH. As seen from Figure 9, using series impedance Zo3, the phase margin at the intersection frequency is increased from PM_2 = 12.2° to PM_1 = 46.8°, meeting the PM requirements > 45°.

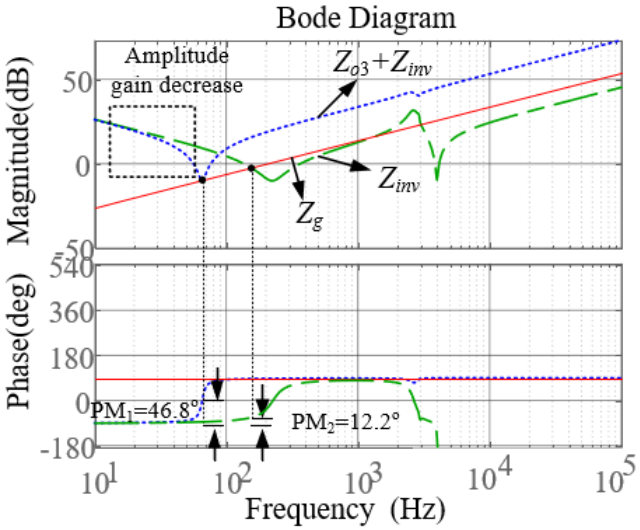

Figure 9. Series impedance correction Bode diagram.

The system control block diagram after series impedance correction is shown in Figure 10.

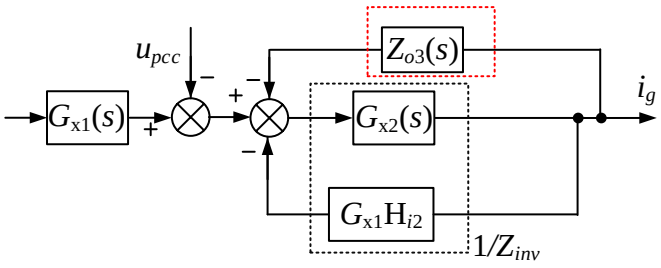

Figure 10. Series impedance control block diagram.

In order to make the control more convenient, the virtual impedance action point is moved forward to the duty cycle d_y.

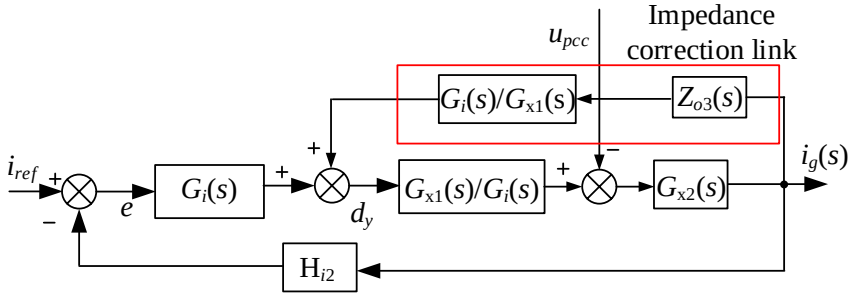

Figure 11. Equivalent transformation diagram.

2.2.2. Feed forward control

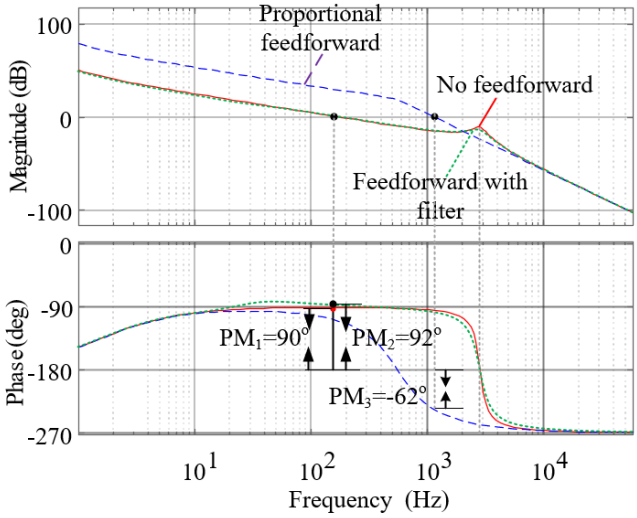

Figure 12. Feedforward link characteristics.

The series impedance correction may successfully increase the system's stability margin, but the amplitude gain of the system in the low frequency region is dropped just after series impedance correction, according to the assessment in Section 2.2.1 and Figure 9. The feed forward control with high gain at low frequency is used to guarantee that the system has adequate amplitude gain [26,27].

Feed forward control can adopt proportional feed forward, feed forward with filter and other forms. As shown in Figure 12, although proportional feed forward is simple used, it feeds back signals in all frequency bands and has the disadvantage of phase delay. However, feed forward with filter has low-pass characteristics and can effectively reduce the interference of high-frequency signals to the system. Therefore, a filter is introduced in the feed forward link. Since the second-order generalized integrator only has high gain for the signal at 50 Hz and very small gain at other frequency harmonics, the filter of the feed forward link adopts the second-order generalized integrator.

The expression of the second-order generalized integrator is shown in Eq (16).

$$G_f(\mathrm{s}) = K * \frac{k_r w_0 s}{s^2 + k_r w_0 s + w_0^2} \tag{16}$$

where K denotes the proportional coefficient of feed forward link, k_r represent a resonance depth, and w_0 is the fundamental frequency.

Figure 13 shows the bode diagram after introducing feedforward, which requires the gain of the system at 50 Hz to be greater than 20 dB. The value of k_r is 0.2. We can clearly observe from the Figure 13 that the amplitude gain of the system is 4.7 dB when feedforward control is not introduced. By constantly trying K, when K = 0.2, it meets the requirement that the system amplitude gain is greater than 20dB.

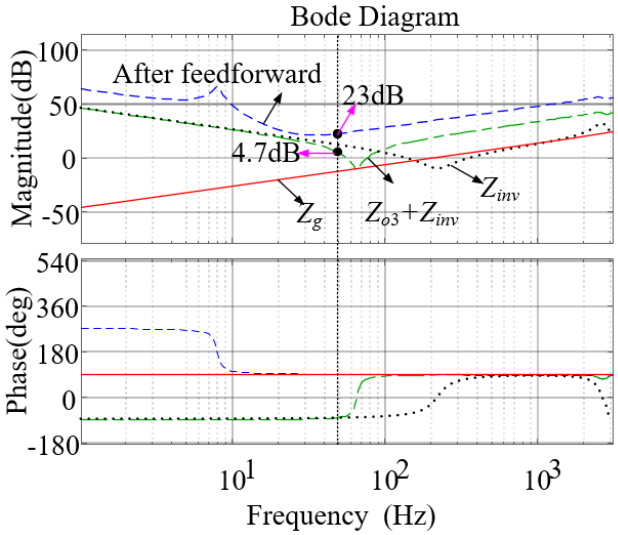

Figure 13. Bode diagram after introducing feed forward.

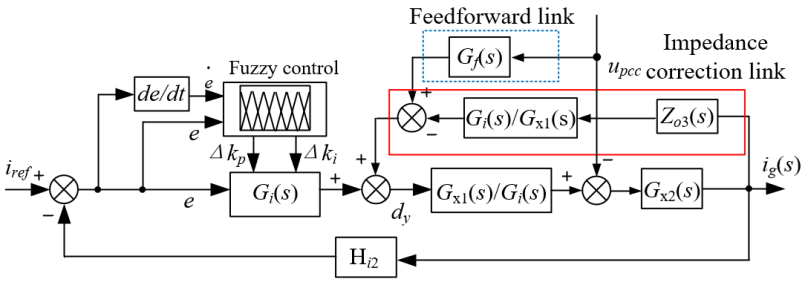

Figure 14. Control block diagram after impedance correction and feedforward.

The control block diagram of adding feed forward link and impedance correction link is shown in Figure 14, in which the series impedance correction link is in the solid frame and the feed forward link is in the dotted frame.

From the above analysis, we can clearly observe that fuzzy control is effective in improving the stability of GTI under low network impedance. but under the condition of high network impedance, AFPIC cannot meet the requirements of system stability margin. In contrast, series impedance correction can improve the system stability margin under high network impedance. Feed forward control can effectively improve the amplitude gain of a low-frequency band of the system. The combination of series impedance correction and feed forward control makes the system obtain good phase margin and amplitude gain. It effectively improves the adaptability of AFPIC to the weak power grid.

3. Results

3.1. Simulation analysis

To check the effectiveness and rationality of the theoretical design in this paper, the simulation model is built using Matlab/Simulink software. The parameters of system under study are listed in Table 2.

Table 2. system parameters.

Parameter	Value
u_{in}/V	500
u_g/V	220
L_1/uH	360
L_2/uH	300
C/uF	10
H_{i1}	1
H_{i2}	0.15

To validate the theoretical analysis, one groups of experiments are used in the simulation, The experimental value of the other group is SCR = 3, and the calculated L_g = 4.6mH.

Judge whether the system operates stably according to the d-axis current: if the d-axis current fluctuates slightly and is basically a straight line, the system operates stably; If the fluctuation range of d-axis current is large, the system will be unstable.

We can clearly observe from Figure 15(a) that under the independent action of fuzzy adaptive PI, the current of d-axis without line inductance is approximately a straight line, and the amplitude of d-axis current is about 25 A after Lg is input, the system is seriously unstable. Figure 15(b) shows the current waveform. We can clearly observe that after the line inductance is input, the system is unstable and the current is seriously distorted.

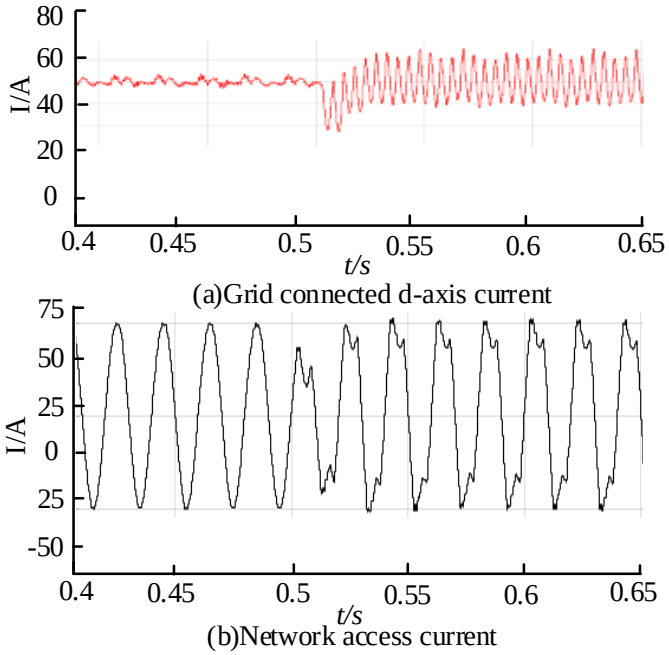

Figure 15. Waveform diagram of network access current when L_g = 4.6 mH.

Figure 16 shows the current waveform of after impedance correction and feedforward. The GTI system operated under strong current network 0.5 s ago, and the inductance L_g = 4.6 mH was input at 0.5 s. We can clearly observe from Figure 16(a) that even if a large line inductance was input, the d-axis current remained in a straight line after series impedance correction and feedforward control, and the system showed good stability. Moreover, the line inductance of L_g = 4.6 mH does not affect the quality of grid-side current, meeting the standard.

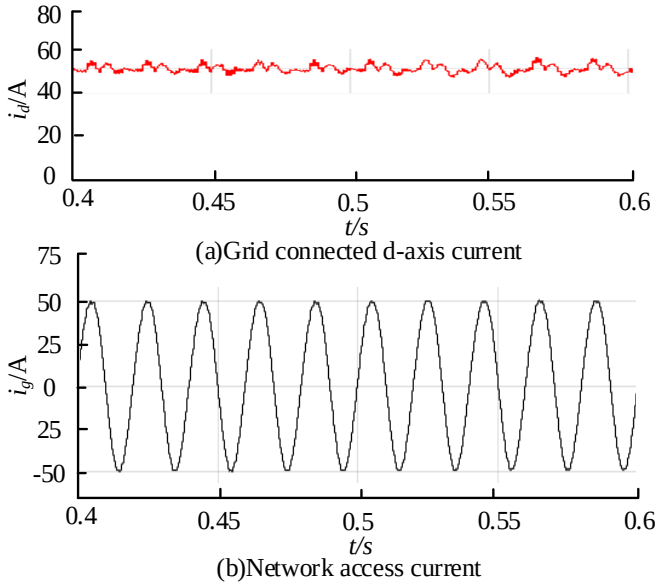

Figure 16. Network current waveform after series impedance correction.

3.2. Experimental verification

An experimental platform is built to verify the method's correctness further. The control chip adopts TMSF28335, the driving chip adopts HCPL-3120, the isolation chip adopts WRB1205s-3WR2, and the switch tube adopts CSD19535. Figure 17 shows the 1kW experimental platform.

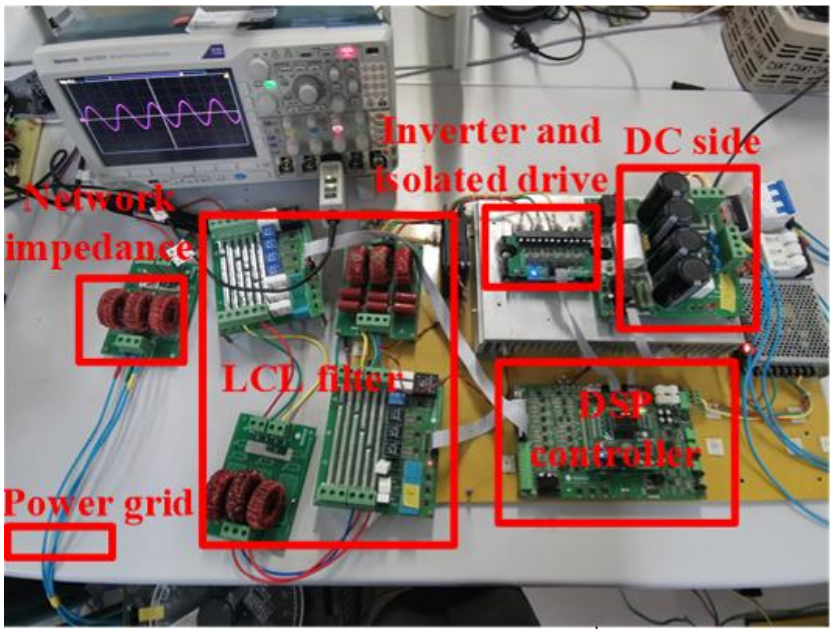

Figure 17. Experimental platform.

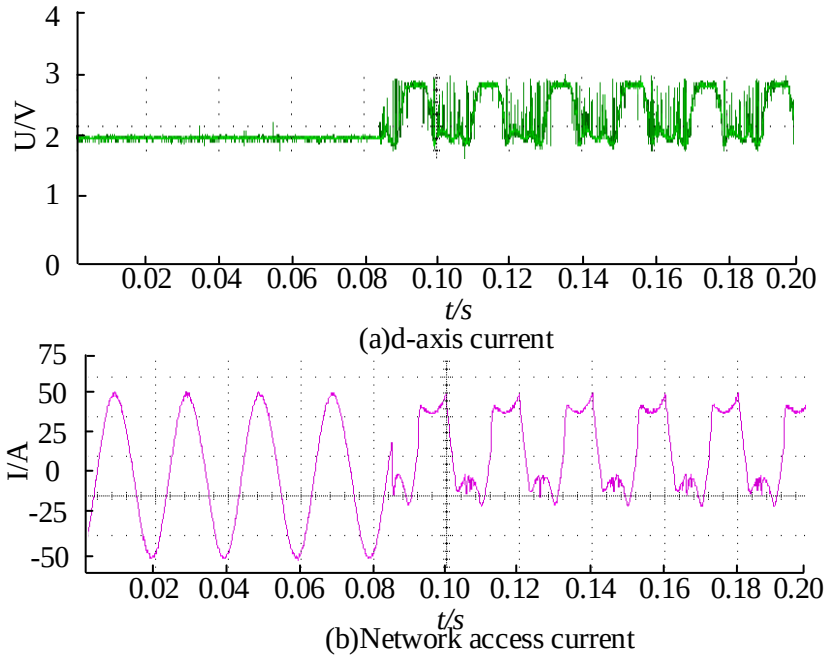

Figure 18. L_g = 4.6 mH experimental waveform.

To make the impedance correction effect more intuitive, the DAC function of DSP is used to output the d-axis current. However, because the DAC function cannot directly output the current, the d-axis current is converted into voltage in equal proportion, in which 1 V voltage corresponds to 25 A current.

To verify that the proposed method still has good control effect under high network impedance, the network impedance of L_g = 4.6 mH is input at 0.1 s. We can clearly observe from Figure 18 that after the network impedance is input, the amplitude fluctuation of d-axis current is about 1 V, the corresponding current is 25 A, the system loses stability, and the network current is seriously distorted.

After series impedance correction and feedforward control, the network current waveform is shown in Figure 19. At 0.1 s, the inductance of L_g = 4.6 mH is input. As can be seen from Figure 19(a), after impedance correction, the d-axis current is still a straight line, and the system remains stable. According to the experimental results in Figure 19, the proposed method still has good stability at high network impedance (SCR = 3), and effectively improves the adaptability of AFPIC to weak power grid.

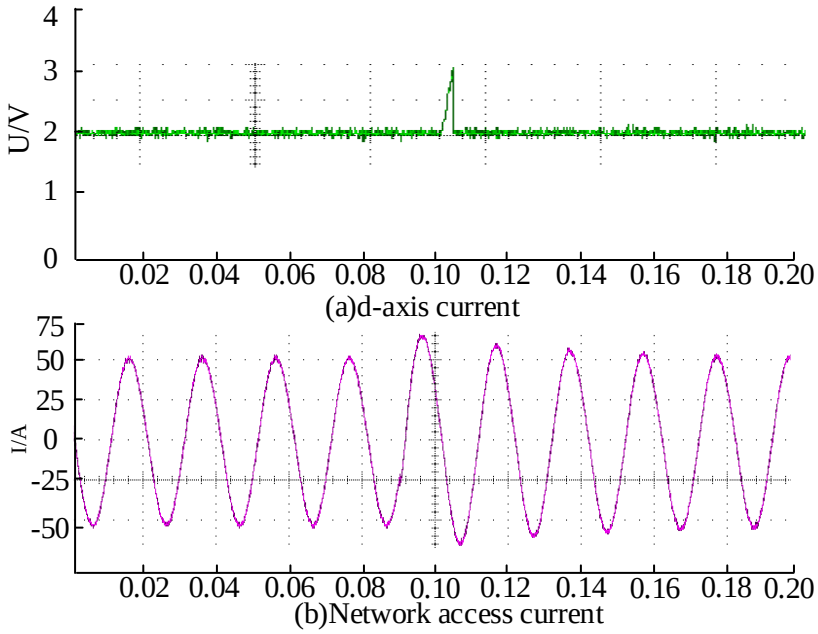

Figure 19. Experimental waveform after impedance correction and feed forward.

4. Conclusions

During regenerative braking in a tram, the large network impedance reduces the stability of the inverter. AFPIC can better ensure the system's stable operation under the condition of low network impedance. Still, under high network impedance, AFPIC cannot meet the requirements of system stability margin, resulting in the instability of GTI. Therefore, the series impedance correction method has been adopted in this paper. The simulation and experimental results showed that under high network impedance, that is, when SCR = 3, the oscillation of AFPIC can reach 25 A, and the system is seriously unstable. The proposed method effectively eliminates the oscillations of AFPIC and greatly improves the stability margin of the GTI system. The advantage of this paper is that the impedance

parameters in series required by the current system can be designed according to the size of the line impedance and the given stability margin, so that the margin compensation of the system has a theoretical basis, the parameters of the series impedance are more accurate, and the compensation effect is better. In the follow-up study, it is also necessary to consider that when the line impedance changes in real time, the series impedance should be able to be adjusted online to follow the change of line impedance, so that the control system can better adapt to the dynamic changes of the system.

Acknowledgments

This research work was supported by Taif University Researchers Supporting Project number (TURSP-2020/144), Taif University, Taif, Saudi Arabia.

Conflict of interest

The authors declare there is no conflict of interest.

References

1. Y. He, K. M. Kockelman, K. A. Perrine, Optimal locations of US fast charging stations for long-distance trip completion by battery electric vehicles, *J. Cleaner Prod.*, **214** (2019), 452–461. https://doi.org/10.1016/j.jclepro.2018.12.188
2. V. A. Kleftakis, N. D. Hatziargyriou, Optimal control of reversible substations and wayside storage devices for voltage stabilization and energy savings in metro railway networks, *IEEE Trans. Transp. Electrif.*, **5** (2019), 515–523. https://doi.org/10.1109/TTE.2019.2913355
3. E. Samavati, H. R. Mohammadi, An improved method for harmonic mitigation and stability improvement of the grid-connected inverters under local load variation and weak grid condition, *Int J. Electr. Power Energy Syst.*, **123** (2020), 106310. https://doi.org/10.1016/j.ijepes.2020.106310
4. S. Fu, X. Zhang, D. Xu, Improved control method of grid-connected converter based on voltage perturbation compensation under weak grid conditions, in *2019 10th International Conference on Power Electronics and ECCE Asia (ICPE 2019-ECCE Asia)*, (2019), 2586–2591. https://doi.org/10.23919/ICPE2019-ECCEAsia42246.2019.8797350
5. F. Hao, G. Zhang, J. Chen, Z. Liu, D. Xu, Y. Wang, et al., Optimal voltage regulation and power sharing in traction power systems with reversible converters, *IEEE Trans. Power Syst.*, **35** (2020), 2726–2735. https://doi.org/10.1109/TPWRS.2020.2968108
6. Y. Wang, W. Wen, C. Wang, H. Liu, X. Zhan, X. Xiao, et al., Adaptive voltage droop method of multiterminal VSC-HVDC systems for DC voltage deviation and power sharing, *IEEE Trans. Power Del.*, **34** (2020), 169–176. https://doi.org/10.1109/TPWRD.2018.2844330
7. B. Liu, H. Ben, Xi. Zhang, T. Meng, X. Wang, Stabilization of a cascaded AC–DC–DC system with small bus capacitance based on small signal analysis, *IEEE Trans. Ind. Appl.*, **54** (2018), 4650–4659. https://doi.org/10.1109/TIA.2018.2837042
8. W. Zhang, Y. Fang, R. Ye, Z. Wang, Analysis and design of a double fuzzy PI controller of a voltage outer loop in a reversible three-phase PWM converter, *Energies*, **13** (2020), 3778. https://doi.org/10.3390/en13153778

9. T. Hou, C. Y. Zhang, H. X. Niu, Quasi-Z source inverter control of PV grid-connected based on fuzzy PCI, *J. Elect. Sci. Technol.*, **19** (2021), 100021. https://doi.org/10.1016/j.jnlest.2020.100021
10. C. W. Tao, C. M. Wang, C. W. Chang, A design of a DC-AC inverter using a modified ZVS-PWM auxiliary commutation pole and a DSP-based PID-like fuzzy control, *IEEE Trans. Ind. Electron.*, **63** (2015), 397–405. https://doi.org/10.1109/TIE.2015.2477061
11. Y. Dai, L. Zhang, G. Liu, C. Yang, D. Zhang, X. Huang, Prescribed-performance based finite-time adaptive fuzzy control for PV inverter in islanded systems, *Int. J. Electron. Power Energy Syst.*, **133** (2021), 107254. https://doi.org/10.1016/j.ijepes.2021.107254
12. Z. Li, W. Cheng, Q. Xiao, W. Liao, Deadbeat predictive power control with fuzzy PI compound controller and power predictive corrector for PWM rectifier under unbalanced grid conditions, *Int. J. Fuzzy Syst.*, **22** (2020), 1277–1288. https://doi.org/10.1007/s40815-020-00847-4
13. T. Lei, S. Riaz, N. Zanib, M. Batool, F. Pan, S. Zhang, Performance analysis of grid-connected distributed generation system integrating a hybrid wind-pv farm using UPQC, *Complexity*, **2022** (2022), 14. https://doi.org/10.1155/2022/4572145
14. Z. Zheng, N. Wang, Z. Sun, Fuzzy PI compound control of PWM rectifiers with applications to marine vehicle electric propulsion system, *Int. J. Fuzzy Syst.*, **20** (2018), 587–596. https://doi.org/10.1007/s40815-017-0394-y
15. S. Riaz, L. Hui, M. S. Aldemir, F. Afzal, A future concern of iterative learning control: A survey. journal of statistics and management systems, **24** (2021), 1301–1322. https://doi.org/10.1080/09720510.2020.1856421
16. R. Wang, Q. Sun, W. Hu, J. Xiao, H. Zhang, P. Wang, Stability-oriented droop coefficients region identification for inverters within weak grid: an impedance-based approach, *IEEE Trans. Syst.*, **51** (2020), 2258–2268. https://doi.org/10.1109/TSMC.2020.3034243
17. Z. Liu, J. Liu, W. Bao, Y. Zhao, Infinity-norm of impedance-based stability criterion for three-phase AC distributed power systems with constant power loads, *IEEE Trans. Power Electron.*, **30** (2014), 3030–3043. https://doi.org/10.1109/TPEL.2014.2331419
18. J. Xu, S. Xie, LCL-resonance damping strategies for grid-connected inverters with LCL filters: A comprehensive review, *J. Mod. Power Syst. Clean Energy*, **6** (2018), 292–305. https://doi.org/10.1007/s40565-017-0319-7
19. S. Li, X. Li, X. Lee, Weighted average current method for active damping control based on grid voltage feed-forward, *J. Cloud Comput.*, **10** (2021), 1–12. https://doi.org/10.1186/s13677-021-00236-8
20. L. Li, W. Chen, Y. Han, Q. Li, Y. Pu, A stability enhancement method based on adaptive virtual resistor for electric-hydrogen hybrid DC microgrid grid-connected inverter under weak grid, *Electr. Power Syst. Res.*, **191** (2021), 106882. https://doi.org/10.1016/j.epsr.2020.106882
21. Z. Lin, X. Ruan, L. Wu, H. Zhang, W. Li, Multi resonant component-based grid-voltage-weighted feedforward scheme for grid-connected inverter to suppress the injected grid current harmonics under weak grid, *IEEE Trans. Power Electron.*, **35** (2020), 9784–9793. https://doi.org/10.1109/TPEL.2020.2970514
22. Z. Xu, A. Xu, S. Xie, Dual-loop grid current control technique for grid-connected inverter using an LCL filter, *Proc. Chin. Soc. Elect. Eng.*, **29** (2009), 36–41.
23. Y. N. Wang, C. Y. Guo, S. Yang, Non-monotonic characteristics of stability margin of MMC system with the change of inner loop current control bandwidth and its mechanism analysis, *Proc. Chin. Soc. Elect. Eng.*, **42** (2022), 3538–3548.

24. M. F. M. Arani, Y. A. Mohamed, Analysis and performance enhancement of vector-controlled VSC in HVDC links connected to very weak grids, *IEEE Trans. Power Syst.*, **32** (2017), 684–693. https://doi.org/10.1109/TPWRS.2016.2540959
25. D. H. Sun, S. Y. Xu, T. Xu, Q. Guo, J. He, B. Zhao, et al., Definition and index of short circuit ratio for multiple renewable energy stations, *Proc. Chin. Soc. Elect. Eng.*, 4**1** (2021), 497–506. https://doi.org/10.13334/j.0258-8013.pcsee.202112
26. T. Xue, P. Sun, Z. Xu, Q. Luo, Feedforward phase compensation method of LCL grid-connected inverter based on all-pass filter in weak grid, *IET Power Electron.*, **13** (2020), 4407–4416. https://doi.org/10.1049/iet-pel.2020.0897
27. D. Yang, X. Ruan, H. Wu, A virtual impedance method to improve the performance of LCL-type grid-connected inverters under weak grid conditions, *Proc. Chin. Soc. Elect. Eng.*, **34** (2014), 2327–2335. https://doi.org/10.13334/j.0258-8013.pcsee.2014.15.001

AIMS Press